Secondary Instability of Second Mode Disturbances in Hypersonic Boundary Layers

Fei Li, Meelan Choudhari, Chau-Lyan Chang and Jeffery White
Computational AeroSciences Branch, NASA Langley Research Center, Hampton, VA 23681

Email: fei.li@nasa.gov, meelan.m.choudhari@nasa.gov, chau-lyan.chang@nasa.gov, jeffrey.a.white@nasa.gov

ABSTRACT

Second mode disturbances dominate the primary instability stage of transition in a number of hypersonic flow configurations. The highest amplification rates of second mode disturbances are usually associated with 2D (or axisymmetric) perturbations and, therefore, a likely scenario for the onset of the three-dimensionality required for laminar-turbulent transition corresponds to the parametric amplification of 3D secondary instabilities in the presence of 2D, finite amplitude second mode disturbances. The secondary instability of second mode disturbances is studied for selected canonical flow configurations. The basic state for the secondary instability analysis is obtained by tracking the linear and nonlinear evolution of 2D, second mode disturbances using nonlinear parabolized stability equations. Unlike in previous studies, the selection of primary disturbances used for the secondary instability analysis was based on their potential relevance to transition in a low disturbance environment and the effects of nonlinearity on the evolution of primary disturbances was accounted for. Strongly nonlinear effects related to the self-interaction of second mode disturbances lead to an upstream shift in the upper branch neutral location. Secondary instability computations confirm the previously known dominance of subharmonic modes at relatively small primary amplitudes. However, for the Purdue Mach 6 compression cone configuration, it was shown that a strong fundamental secondary instability can exist for a range of initial amplitudes of the most amplified second mode disturbance, indicating that the exclusive focus on subharmonic modes in the previous applications of secondary instability theory to second mode primary instability may not have been fully justified.

1. BACKGROUND AND OBJECTIVE

By virtue of its influence on surface heat transfer, skin friction, and separation characteristics, boundary layer transition from a laminar to a turbulent state tends to dominate the design and performance of hypersonic flight vehicles. At hypersonic Mach numbers, the first mode instability becomes less important or, in many cases, is not a factor in the transition process. For an axisymmetric body at zero angle of attack in a hypersonic flow (as well as in cases where the boundary layer is essentially two-dimensional), the crossflow instability is absent as well. In these cases, the predominant instability mechanism involves the second mode disturbances. The most unstable second mode instability is axisymmetric (e.g. on a cone at zero angle of attack) or two-dimensional (e.g. on a flat plate) in nature. Thus, the oblique breakdown mechanism, which is believed to dominate first mode transition in supersonic flows, becomes less relevant at hypersonic Mach numbers. Therefore, a good and thorough understanding of the breakdown of two-dimensional or axisymmetric second mode waves is essential for understanding this important scenario for transition. Similar to its counterpart in incompressible flows (the Tollmien-Schlichting wave) [1], the second mode wave is susceptible to three-dimensional secondary instability when its amplitude becomes sufficiently large [2,3]. Because the second mode instability and the associated secondary instability in hypersonic flows usually attain frequencies in the range of hundreds of kilo-Hertz to a few mega-Hertz, which is beyond the currently available high-frequency sensors, the computational approach is the only way to study them in detail. The objective of this research is to study the breakdown mechanism via secondary instability of the finite

amplitude second mode by using a combination of 2D-eigenvalue analysis, parabolized stability equations, and direct numerical simulation.

Studies for low-speed boundary layers (see, for instance, [1] and the various references cited therein) have shown that the 3D, secondary instabilities can have much higher amplification rates than those of the underlying primary disturbances and can lead to transition via three generic breakdown mechanisms. The first mechanism corresponding to the so-called fundamental or K-type breakdown is initiated by secondary instability modes that have the same frequency and streamwise wavelength as the 2D primary instability and manifest themselves via a streamwise aligned pattern of lambda-shaped vorticity structures. The second mechanism is the subharmonic or H-type breakdown, which involves secondary instability modes that correspond to one half the frequency and twice the streamwise wavelength as that of the primary instability and lead to a staggered pattern of lambda vortices in flow visualizations. The third type of secondary instability modes are intermediate to the fundamental and subharmonic disturbances in many regards and are known as detuned modes because they are not phase locked to the primary instability wave. Because of the relatively high growth rates of the secondary instabilities, they could also serve as a more robust harbinger of the onset of transition in comparison with the traditionally employed method of linear amplification of primary disturbances. Previously, El-Hady [4] had used the logarithmic amplification factors (i.e., the so called N-factors) associated with the linear amplification of secondary instabilities as a metric to gauge the overall effect of surface cooling on secondary instability growth. Extending that idea, the N-factor for secondary modes could perhaps be used to develop a more robust N-factor correlation with the onset of transition in 2D or axisymmetric boundary layers, especially when the primary instability is dominated by 2D disturbances. Such an approach, along with additional refinements for calculating the growth rates of secondary modes, is pursued in this paper to quantify the growth potential of the different types of secondary instabilities associated with second mode primary disturbances in hypersonic boundary layers. The results obtained for selected canonical high-speed boundary layers are described in Section 2 below. Concluding remarks are presented in Section 3.

2. RESULTS

Three geometric configurations are used for the analysis of secondary instabilities of second mode primary disturbances with finite amplitudes: (1) self-similar boundary layers over flat plates for different Mach numbers, (2) a 0.47 meter long compression cone model with a concave streamwise curvature [5] that was designed for transition tests in the Mach 6 quiet tunnels at Purdue University, and (3) a 1.1 meter long straight circular cone with 7-degree half angle and 2.5 mm nose radius that was flown during the HIFiRE-1 flight experiment [6]. The flat plate boundary layers provide the simplest setting to study the secondary instability phenomenon. They are used to validate the results of the present approach against previous results from the literature as well as to highlight a couple of significant limitations of the previous body of results. The compression cone model was designed to help achieve transition in a quiet environment under constraints on the cone length and base diameter. By virtue of its constant streamwise radius of curvature over most of the cone length and a slower variation in boundary layer stability characteristics than those over a straight cone, the compression cone model introduces certain unique physical effects that are relevant to the secondary instability characteristics. The results in this paper primarily emphasize this compression cone configuration. The HIFiRE-1 cone illustrates the behavior of secondary instability for an in-flight configuration, including the effects of strong surface cooling. Both cone configurations also involve the effects of axially varying transverse surface curvature.

The second mode instability characteristics for the two cone configurations show some differences, among which the most relevant to the secondary instability analysis are those pertaining to the streamwise range of

amplification for a mode of fixed frequency. As described later, the linearly most amplified second mode disturbances remain unstable over nearly the entire length of the compression cone configuration. On the other hand, for the straight cone HIFiRE-1 model, each linearly unstable second mode of a fixed frequency amplifies over a shorter distance before another mode of lower frequency takes over downstream. The latter behavior is also typical of hypersonic flow over a flat plate as well as other straight cones over a range of Mach numbers. The above differences in linear growth characteristics could have a significant impact on the threshold amplitudes of second mode disturbances required to achieve transition over a fixed length model.

A. Validation of Secondary Instability Predictions for Flat Plate Boundary Layers

Secondary instability of second mode instabilities was first studied by Ng and Erlebacher [2] for a Mach 4.5 boundary layer with adiabatic wall. When the spatial growth rate of the primary second mode disturbance is sufficiently small, the change in primary amplitude over a single streamwise wavelength may be assumed to be negligible, so that the basic state comprised of the underlying (and slowly evolving) boundary layer flow plus the primary disturbance may be approximated as locally periodic in a coordinate system that moves with the phase speed of the primary wave. The secondary instability perturbations are then governed by a set of partial differential equations with periodic coefficients in the streamwise direction in the moving frame. As a result, eigenfunction solutions to the resulting set of partial differential equations (PDEs) also take on a specific periodic form [1]. As mentioned in Section I, two special cases of the secondary instability correspond to the fundamental and subharmonic modes with eigensolutions that have, respectively, the same streamwise wavelength and twice the wavelength of the second mode base flow in the laboratory frame. A more general solution can have a wavelength that is not necessarily an integral multiple of the second mode base flow wavelength; this is termed the detuned mode. A parameter ε can be defined to characterize the periodic properties of the secondary instability, with $\varepsilon = 0$ and 1 indicating the fundamental and the subharmonic modes, respectively. For $0 < \varepsilon < 1$, the secondary instability is detuned [1]. For a detailed description of the secondary instability theory and the derivation of the relevant governing equations, the reader is deferred to [1–3].

The base flow in the earlier analyses [2–4] of secondary instabilities of second mode disturbances was composed of simply a second mode linear eigenfunction with a small but finite amplitude superimposed on the self-similar laminar boundary layer flow, i.e., the effects of nonlinear self-interaction on the second mode primary instability were not accounted for. As shown later in this paper, second mode disturbances can achieve rather substantial amplitudes approaching root-mean-square streamwise velocity fluctuations in excess of 10 percent of the free-stream velocity (i.e., peak velocity fluctuations approaching 15 percent). Thus, we employ a more general formulation that allows one to retain an arbitrarily large number of harmonics of the nonlinear second mode disturbance and, correspondingly, an equal or larger number of Fourier modes in the secondary instability field as well. The nonlinear evolution of the second mode (primary) instability is predicted using the nonlinear version of the parabolized stability equations (PSE) or via direct numerical simulation. The resulting eigenvalue problem for 3D secondary instabilities is solved using a partial differential equation based planar eigenvalue solver that was first developed in the context of secondary instability of stationary crossflow vortices [7]. Depending on the objective of the calculation, the eigenvalue problem may be solved for the temporal eigenvalue or the spatial one. To allow efficient N-factor computations for the secondary instability modes, the temporal eigenvalue problem is solved in this paper and the temporal growth rate is converted to spatial growth using Gaster's transformation, analogous to [2]. Spot checks using purely spatial computations have confirmed the satisfactory accuracy of this approach. (See [1] for similar findings in the case of incompressible boundary layers.) However, further work is under way to establish the effects of the temporal approximation in a more thorough fashion.

As a validation of the modified computational approach for secondary instability analysis, computations were performed for the Mach 4.5 flat-plate boundary layer configuration from [2], and the agreement between the previous results and the results computed via the modified version of the planar PDEbased eigenvalue solver from [7] is very good (Fig. 1(a)). Additional comparisons of a similar nature were obtained for secondary instability of first modes waves in the same Mach 4.5 boundary layer (Fig. 1(b)), as well as for the fundamental mode of secondary instability in a Mach 1.6 boundary layer (Fig 1(c)). The Mach 1.6 results were used for comparison because [2] did not find any significant fundamental secondary instability at the highest Mach number (Mach 4.5) considered in that paper. In general, there may be more than one family of unstable secondary disturbances, but only the dominant family of modes in any given context is considered in this paper.

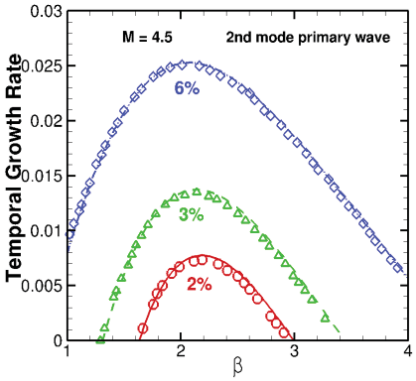

(a) Subharmonic instabilities of a 2D second mode primary wave in a Mach 4.5 boundary layer. The red, green, and blue curves denote increasing local amplitudes of the primary wave (2%, 3%, and 6%, respectively).

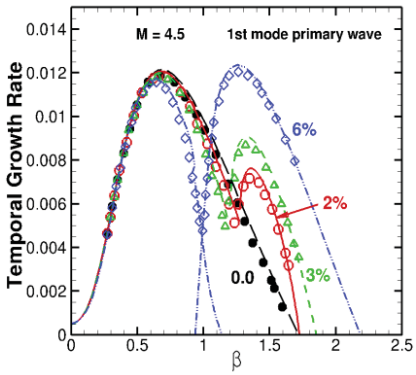

(b) Subharmonic instabilities based on 2D first mode wave in a Mach 4.5 boundary layer.

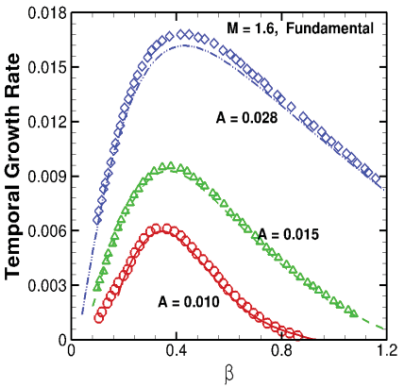

(c) Fundamental modes of secondary instability based on 2D first mode wave in a Mach 1.6 boundary layer

Figure 1. Comparison of secondary instability growth rates with the results of Ref. 2 for Mach 4.5 and Mach 1.6 boundary layers over a flat plate with adiabatic conditions. The temporal growth rate is plotted against spanwise wavenumber β. Lines denote present results, whereas symbols in parts (a) through (c) indicate results from Figs. 12, 11, and 9, respectively, in [2]. Details of flow conditions and normalization of temporal growth rate and β are given in [2].

The second mode amplitudes as reported in [2] (and, also, as indicated in Fig. 1(a)) are based on the amplitude of the normalized temperature fluctuation T'/T_∞. In this particular case, the velocity amplitude u'/U_∞ is approximately 15 times smaller than the temperature based amplitude and, therefore, is less than 1 percent even for the highest amplitude case (6 percent amplitude based on temperature) considered in [2]. As noted later in the context of the compression cone, an order of magnitude larger amplitude can arise in the course of the nonlinear development of second mode disturbances and, furthermore, can alter the growth characteristics of second mode instabilities. For example, at the low amplitudes considered in [2], the fundamental modes of secondary instability are either stable or amplify at negligible rates; however, although not shown in this paper, the fundamental modes of second mode primary disturbances do come into play when the second mode amplitude is increased beyond the levels considered in Fig. 1(a) and quickly achieve growth rates that are comparable to those of the subharmonic modes. Additional discussion of this phenomenon is provided in the following subsection pertaining to the compression cone, wherein the evolution of secondary disturbances is followed concurrently with the primary mode (compared to the local analysis in [2]).

The secondary instability results presented in [2] were limited to isolated streamwise stations and, furthermore, the selection of primary disturbance did not explicitly consider which second mode frequency might dominate the initial stage of transition. While [3] did include some results including the integrated amplification of secondary disturbances, the selection of the primary disturbance again appears to be somewhat arbitrary and, hence, the earlier body of results may be more relevant to artificially excited primary modes in a laboratory experiment rather than to natural transition in a broadband disturbance environment. The identity of the dominant primary disturbance in the natural environment would be determined, to a significant extent, by the linear amplification characteristics of the unperturbed laminar flow, assuming that the disturbance environment and the receptivity characteristics (as well as the nonlinear interactions) do not exhibit a strong spectral selectivity across the bandwidth of primary disturbances. Besides accounting for the filtering action of the linear amplification stage, the results presented in this paper account for the effects of nonlinearity on the development of the primary disturbance, allowing the secondary instability analyses to be extended to a substantially larger range of primary amplitudes than the previous literature.

B. Mach 6 Compression Cone

The second flow configuration studied herein corresponds to the Purdue Mach 6 compression cone [5] with a stagnation pressure of 930.1 kPa, a stagnation temperature of 426.0 K, and unit Reynolds number of 10.8×10^6 per meter. The cone is 0.47 meters long and has a constant surface radius of curvature equal to 3 meters in the axial direction. It tangentially joins a small nose sphere of radius 0.16 mm at an initial half-angle of 1.4 degrees. The boundary layer over this surface is susceptible to modest Görtler and first mode instabilities and a strong second mode instability that is known to dominate the primary instability stage on this model (see, for instance, [8]). Accordingly, the secondary instability of the second mode waves is studied herein. Initial results for this case were presented in [8]. Besides the secondary instability route, however, there exist multiple other scenarios for transition over this compression cone model, namely,

(i) Görtler-2nd mode interactions, shown to be capable of inducing transition for rather small initial amplitudes [9],

(ii) Oblique 2nd mode interactions, which were found to result in later transition for initial amplitudes comparable to those in (i) above [9]

(iii) Oblique breakdown involving first mode disturbances, which is unlikely to cause transition because of the weak first mode instability

(iv) Secondary instability of Görtler vortex instabilities [9] which, again, is less likely except in the case of strong excitation of Gortler modes via large amplitude surface non-uniformities, and

(v) Interactions between oblique first mode and axisymmetric second mode, which are unlikely due to the disparity between first mode and second mode frequencies.

Whether or not the secondary instability of second mode disturbances will dominate the other scenarios in practice will depend, in part, on the initial spectrum of the various types of instability waves in the boundary layer flow over the compression cone.

Mean flow computations for the cone models are carried out using the NASA developed Navier-Stokes solver VULCAN [10]. Linear and nonlinear growth of the primary, second mode disturbances is computed using parabolized stability equations (PSE) as implemented within the NASA developed LASTRAC code [11] and linear growth characteristics of secondary instability modes are predicted using a modified version of the numerical framework from Ref. [7] as mentioned previously. The base flow for secondary instability incorporates all dominant harmonics of the second mode instability, including distortion, if any, of the primary (i.e., fundamental) harmonic.

Nonlinear Evolution of Axisymmetric Second Mode Waves

Figure 2(a) shows the N-factor evolution for axisymmetric second mode disturbances (i.e., with an azimuthal wave number of n=0) of various frequencies as predicted by linear PSE. It is seen that modes in the neighborhood of 300 kHz frequency are most amplified over the aft portion of the cone. It is well known that a 2D or axisymmetric second mode is more unstable than an oblique second mode of the same frequency. This is confirmed in Fig. 2(b), where the N-factors for second mode disturbances at 300 kHz but nonzero azimuthal wavenumbers have been plotted. Fig. 2(b) underscores the dominance of the axisymmetric second mode disturbances throughout the region of instability. It is also interesting to note that all of the N-factor curves in Fig. 2(a) and (b) are monotonically increasing (indicative of a sustained growth of second mode disturbances with frequencies near 300 kHz), and a maximum N-factor of 19 is reached at the end of the cone, indicating very strong second mode growth. This behavior is rather different from the linear amplification characteristics for the straight cone (Fig. 2(c)), where a second mode disturbance at any given frequency gets amplified over a relatively short fraction of the body length, so that the frequency of the most amplified disturbance changes more rapidly along the length of the cone.

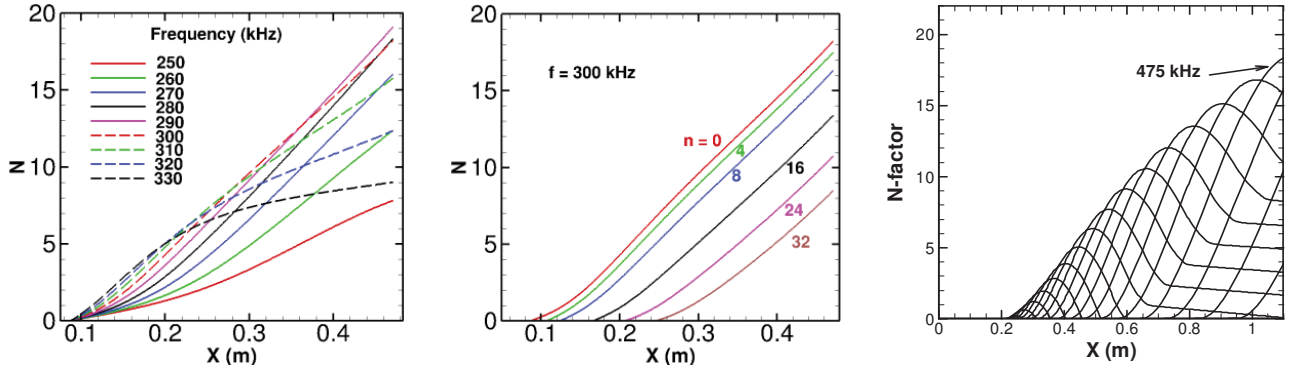

(a) Compression cone, N-factors of axisymmetric second mode disturbances at various frequencies.

(b) Compression cone, N-factors for oblique second mode disturbances at 300 kHz.

(c) HIFiRE-1 cone, N-factors of axisymmetric second mode disturbances at various frequencies.

Figure 2. Linear N-factors of second mode disturbances for cone models of interest

Next, the nonlinear growth of second mode perturbations is investigated using nonlinear PSE calculations for six different initial amplitudes of the axisymmetric second mode disturbance with a frequency of 300 kHz. Figure 3 displays the streamwise evolution of the modal amplitude corresponding to the fundamental harmonic in each case. The corresponding evolution of the mean flow distortion component is also indicated via the dashed curves in the figure. It is well known that nonlinear effects will come into play as the disturbance amplitude increases, and the second mode evolution will begin to depart from the linear theory prediction. As a result of nonlinearity, one would expect the fundamental mode amplitude to saturate eventually and, hence, grow and/or decay in a slower (i.e., algebraic) fashion. However, a somewhat different behavior is observed for the particular case under discussion. Specifically, the fundamental amplitude decreases rapidly after achieving a peak amplitude of approximately 15 percent of the free-stream velocity, and the rates of decay are comparable to the preceding rates of exponential growth. Effectively, the increased nonlinearity brings the upper neutral branch to an increasingly forward location as the initial disturbance amplitude is increased. The dashed curves in Fig. 3 also indicate that the mean flow correction term does not decay as rapidly as the fundamental and remains at relatively large amplitudes for considerably longer distance. These nonlinear results indicate that the second mode disturbance becomes stable for the strongly modified mean state, as an outcome of the nonlinear interactions among all harmonics.

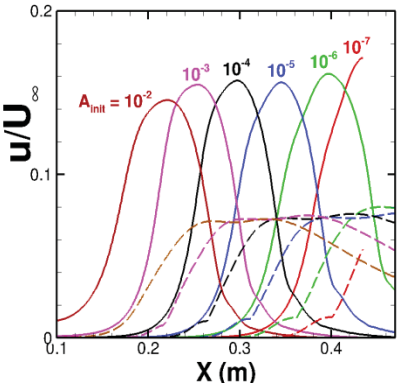

Figure 3. Nonlinear growth of the peak amplitude of selected Fourier harmonics of second mode disturbance for selected initial amplitudes A_{init}. (Solid curves: fundamental, dashed curves: mean flow distortion)

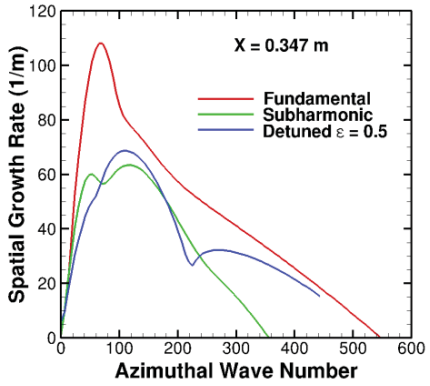

Figure 4. Growth rates of secondary instability modes at a fixed streamwise location. Initial amplitude of the primary second mode wave is equal to 10^{-5}.

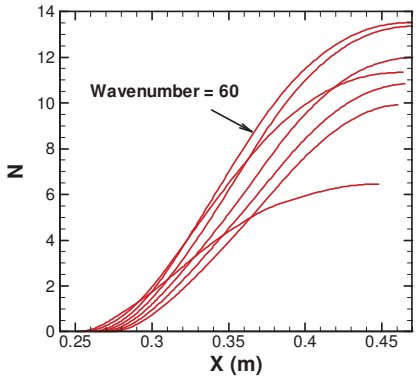

(a) Fundamental secondary instability.

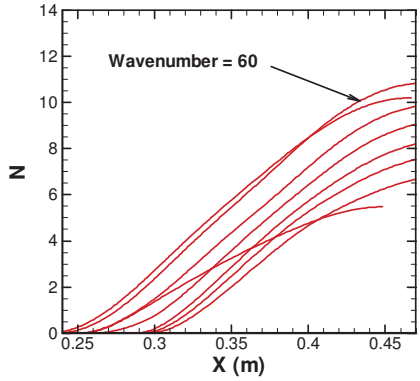

(b) Subharmonic secondary instability.

Figure 5. Linear N-factors of secondary instability for initial second mode amplitude of 10^{-5}. Azimuthal wavenumbers range from 20 to 140 for fundamental mode and from 20 to 160 for subharmonic mode, in increments of 20.

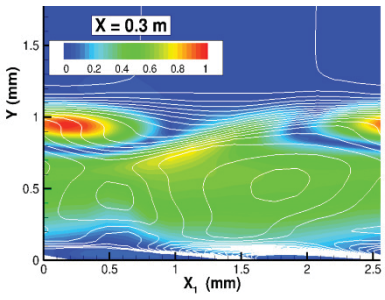

(c) Fundamental

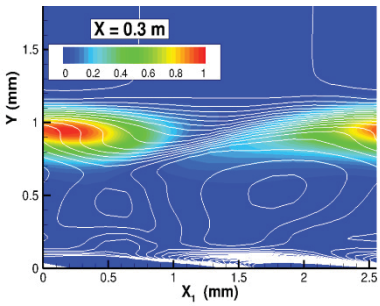

(d) Subharmonic

Figure 5 (continued). Eigenfunction shapes of streamwise velocity fluctuations. The abscissa X_1 denotes local streamwise coordinate, measured relative to the station where the secondary analysis is carried out (X = 0.3 m), whereas the ordinate corresponds to the wall-normal direction. The range of X_1 corresponds to one spanwise wavelength of the secondary instability mode. The background white lines represent contours of mean shear dU/dy. The base flow is from left to right.

Figure 4 shows the results of secondary instability analysis for an axisymmetric second mode disturbance of frequency 300 kHz and an initial amplitude of $A_{init} = 10^{-5}$. Throughout this paper, the second mode amplitude is measured in terms of the streamwise velocity fluctuation normalized by the free-stream velocity, except in the course of comparison with previous results in Fig. 1(a), where the amplitude of the temperature fluctuation was used to maintain consistency with [2]. The initial amplitude A_{init} corresponds to the initial marching location, i.e., the approximate neutral location where the second mode disturbance first begins to amplify. The growth rates of secondary instability modes are computed using the nonlinear PSE solution as the base flow. Figure 4 shows the local streamwise growth rate as a function of the azimuthal wavenumber for three different modes of secondary instability, namely, a fundamental, a subharmonic and a detuned ($\varepsilon = 0.5$) mode. The streamwise location corresponds to $x = 0.35$ m, which is near the peak of the second mode amplitude during its nonlinear evolution. The fundamental mode has the highest growth rate at this location, while the subharmonic and the detuned modes have comparable growth rates. The unstable spectra span a wide range of azimuthal wavenumbers (n) with peak growth at approximately $n = 60$ for the fundamental mode. All three types of secondary instability are approximately phase locked with the second mode primary instability.

N-factor computations of both fundamental and subharmonic modes of the secondary instability were carried out for a selected set of azimuthal wavenumbers (Fig. 5). For both types of secondary instabilities, the $n = 60$ mode appears to dominate the secondary growth over most of the region. With a maximum N-factor of 13.5 for the fundamental mode and approximately 11 for the subharmonic mode, a strong secondary instability growth is indicated. Fig. 5(c) and 5 (d) show, respectively, the shapes of the fundamental and subharmonic eigenfunctions in terms of colored contours of the streamwise velocity fluctuation, while the background white lines are contours of the mean streamwise shear. The nearly horizontal band of background white lines in Fig. 5(c) and 5(d) indicate the concentration of strong shear created by a finite amplitude second mode, which coincides with the maximum amplitudes of secondary instability.

The axial evolution of the spatial growth rate corresponding to both modes of secondary instability is shown in Fig. 6. It may be seen that the fundamental mode becomes unstable slightly farther downstream and also reaches its upper branch neutral location somewhat earlier, indicating a higher threshold for the amplitude of the primary wave. However, the fundamental mode exhibits substantially stronger growth rates (almost twice as large) than the subharmonic mode in the vicinity of X = 0.35 m, where the primary disturbance achieves its peak amplitude. The peak growth rate of the fundamental mode is approximately twice the peak growth rate of the primary mode although, of course, the growth rate variation of the fundamental mode lags behind the growth rate variation for the primary disturbance. Throughout the region of instability corresponding to both fundamental and subharmonic modes (except in the immediate vicinity of the upper neutral branch for the secondary, where the primary disturbance is decaying rapidly), the primary disturbance grows (or decays) by less than 10 percent across a single wavelength. Indeed, when the secondary growth rates are at their highest, the primary growth (or decay) rate is much smaller in magnitude. This provides some a posteriori support for freezing the amplitude of the primary disturbance during the secondary instability analysis. Additional justification is provided in the latter part of this subsection via a comparison between the secondary instability predictions and PSE computations for the subharmonic modes.

Although not highlighted within Figs. 5(a) and 5(b), secondary instability modes at neighboring azimuthal wavenumbers also achieve rather high amplification factors, very close to those of the $n = 60$ modes. The wave angles for the subharmonic (and fundamental) disturbances with $n = 60$ vary from approximately 70 degrees at their onset near X = 0.25 m to about 30 degrees near the end of the cone. The variation of the secondary N factors with azimuthal wavenumber at selected axial stations is shown in Fig. 7(a). The

corresponding variation in local growth rates of the secondary disturbances is shown in Fig. 7(b). According to Fig. 7(a), the peak N-factor for the fundamental modes of secondary instability occurs at a somewhat larger n than the corresponding value for the subharmonic mode. However, the N-factor spectrum for both types of modes is rather broad, as disturbances from $n \approx 40$ to $n \approx 100$ achieve Nfactors of N_{max} -2 or greater for the fundamental secondary mode, and a similar behavior is observed for subharmonic modes between $n \approx 30$ and $n \approx 90$. Here, N_{max} denotes the peak N-factor achieved by a fixed frequency instability mode over the entire length of the cone.

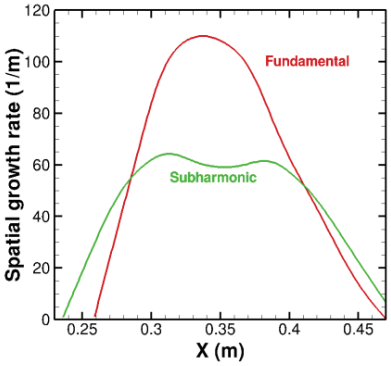

Figure 6. Spatial growth rate as a function of axial location for an azimuthal wavenumber of n = 60.

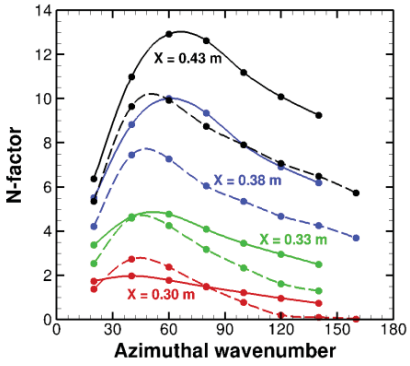

(a) N-factor spectrum

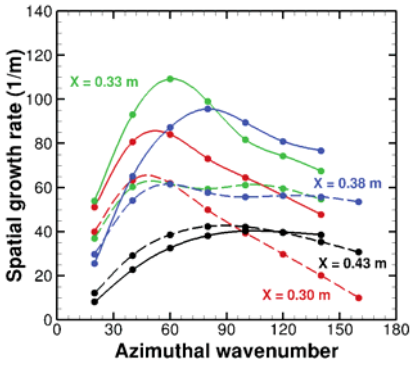

(b) Growth rate variation

Figure 7. Azimuthal wavenumber spectra of secondary instability at selected streamwise stations. (Solid lines: fundamental mode; dashed lines: subharmonic mode. Each curve indicates spline fit through the computed points shown with symbols.)

Next, the effect of the initial amplitude of the second mode primary wave on the amplification characteristics of the secondary instability is studied for a primary second mode disturbance of frequency 300 kHz and an initial amplitude A_{init} of 10^{-4}. This parametric variation is also expected to provide some insights into the effects of the earlier stage of transition (namely, the combined effect of external disturbance environment and the receptivity characteristics for second mode waves) on the ensuing transition process. It is found that the fundamental mode is still dominant, but the maximum N-factors reached for both the fundamental and subharrmonic modes are slightly lower, and the peak wavenumber of the subharmonic mode is shifted to $n \approx$ 40 (Fig. 8).

The linear secondary instability theory used here does not account for the effects of mean flow non-parallelism and the surface curvature in both longitudinal and transverse directions. On the other hand, a PSE computation includes both of these effects. Furthermore, nonlinear PSE computations can trace the nonlinear evolution of secondary instability up to the onset of transition. To gauge those effects, nonlinear PSE computations were initiated for a second mode of frequency 300 kHz and an initial amplitude of 10^{-4} at approximately x = 0.095 m, and a subharmonic secondary instability mode of n = 80 is inserted when the nonlinear PSE marching reaches x = 0.26 m, slightly downstream of the neutral point of this secondary instability mode. It is also noted that, near the neutral point at $x \approx$ 0.26 m, the root mean square (RMS) amplitude of the primary wave is approximately 0.011.

Figure 9 shows the nonlinear evolution of modal amplitudes of the second mode (red lines) and the secondary instability (green lines) downstream of X = 0.26 m. Also plotted in Fig. 9 is the secondary instability amplitude predicted by linear theory, which is represented by solid black dots. Initially, the linear theory agrees well with the nonlinear PSE results, despite its lack of non-parallelism and curvature effects. Eventually, however, somewhat larger differences begin to appear between the secondary instability theory and the PSE computations, presumably due to nonlinear effects as the secondary disturbance overtakes the primary disturbance in amplitude near X = 0.42 m. Similarly, Fig. 10 shows a comparison between the streamwise evolution of peak RMS amplitude of the secondary instability at a given station and the corresponding prediction from linear secondary instability theory.

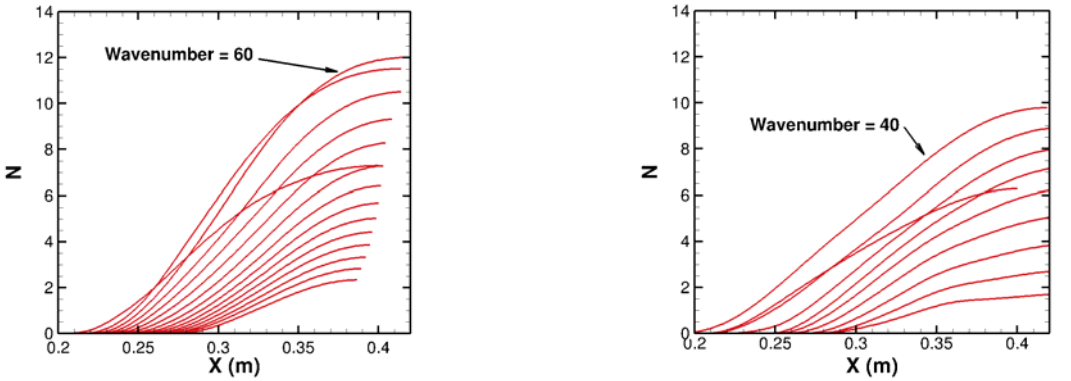

(a) Fundamental secondary instability. **(b) Subharmonic secondary instability.**

Figure 8. N-factors for fundamental and subharmonic modes for a primary wave of initial amplitude 10^{-4}. Azimuthal wavenumbers range from 20 to 300 for fundamental mode and from 20 to 200 for subharmonic mode, in increments of 20.

The onset of transition is often characterized by a sharp rise in the mean wall shear. The evolution of mean wall shear in the presence of secondary instabilities of various initial amplitudes is shown in Fig. 11. The wall-shear curve with only the second mode present (no secondary instability) is shown in black and serves as a reference for determining the onset of transition or, at least, the location of significantly increased shear stress due to the secondary disturbances. For the secondary instability with the smallest initial amplitude (the red curve), the wall-shear follows the reference curve for most of its history, but begins to rise at $x \approx 0.44$ m, just before the end of the cone is reached. This does not necessarily indicate the onset of transition, but certainly signifies the onset of a strongly nonlinear behavior. The curve corresponding to the larger initial amplitude of the subharmonic mode begins to deviate slightly from the reference curve before rising sharply at $x \approx 0.40$ m.

Fig. 12 shows the RMS contours of streamwise velocity fluctuations of secondary instability at three selected cross-sections on the cone for the initial subharmonic amplitude of 10^{-5}. Initially, the RMS contours consist of large islands near the edge of the boundary layer. As the onset of strongly nonlinear effects near $x \approx 0.44$ m is approached, these islands begin to break up into smaller scales.

The results in this subsection indicate that subharmonic secondary instability is a viable route to transition in the compression cone boundary layer. Since the fundamental modes of secondary instability appear to have a higher linear growth potential than the subharmonic modes, it will be important to determine their role in transition. It may be noted that the subharmonic secondary instability does not involve a strong, stationary vortex component and, therefore, may not account for the stationary vortex signature seen from the experimental visualization of the surface flow via temperature sensitive paint (TSP) [6]. As pointed out in

Ref. [8], however, the fundamental mode of secondary instability does involve an O(1) stationary vortex component as part of its mode shape and, hence could possibly account for the abovementioned stationary vortices seen in the TSP images. The validity of this earlier proposal is borne out by the findings of the subsequent numerical simulations in [12].

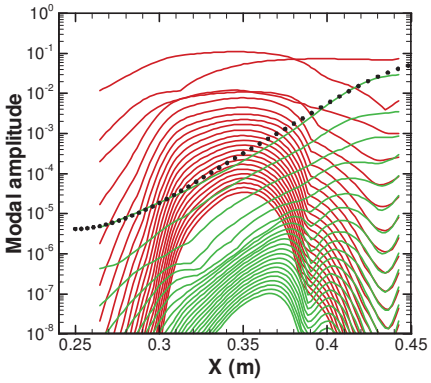

Figure 9. Evolution of second mode (red) and subharmonic secondary instability (green) as computed via nonlinear PSE. (Black dots: linear theory)

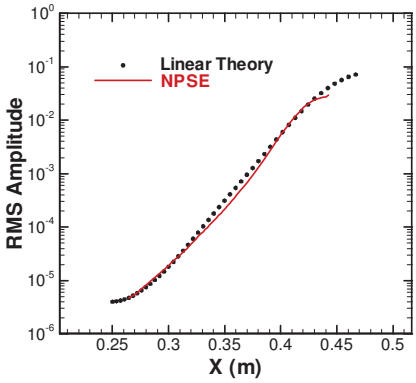

Figure 10. Comparison of RMS amplitude of secondary instability computed by nonlinear PSE and linear theory, respectively.

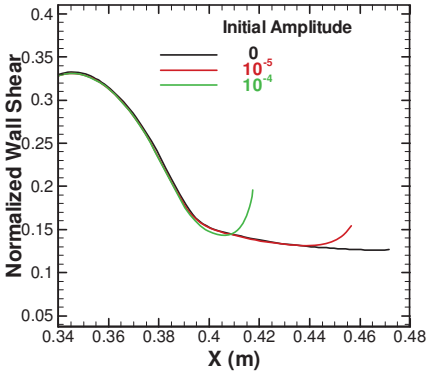

Figure 11. Evolution of normalized wall-shear for various initial amplitudes of secondary instability.

In practice, the relative importance of fundamental and subharmonic modes depends both on their linear amplification characteristics and the initial amplitudes. Nonlinear interactions between second mode disturbances (i.e., mode (1,0), where the first and second indices correspond to temporal and azimuthal harmonics relative to the fundamental) and a stationary vortex structure (mode (0,1)) excites the oblique mode (1,1) that can begin to amplify at a rapid rate through the process of parametric resonance. Such direct (and strong) excitation of the fundamental modes via stationary streamwise vorticity in the flow can lead to effectively higher initial amplitudes of the fundamental modes, helping them dominate the early phase of the nonlinear development. Indeed, in certain low-speed flows with streamwise vorticity, fundamental breakdown has been observed in cases where the subharmonic breakdown might have been expected to dominate based on the sole consideration of secondary amplification factors [1]. Thus, the broader picture including the effect of receptivity characteristics must be kept in mind during practical applications of the secondary instability theory.

C. Straight Circular Cone

As described in [13], the linear amplification phase of transition over the HIFiRE-1 model during a portion of the ascent phase is dominated exclusively by second mode disturbances. The most amplified second mode disturbances are again axisymmetric in nature and the amplification ratios (N-factors) decrease rapidly with increasing wave angles with respect to the flow direction. Because transition to turbulence must entail an energy cascade in all three dimensions, a likely catalyst for transition onset may involve the relatively rapid growth of non-axisymmetric secondary instabilities that are supported by finite amplitude second mode waves. These secondary instabilities might originate from oblique second mode disturbances or other 3D

disturbances that are linearly stable. It may be noted that the concave curvature on the compression cone model from the previous subsection is likely to influence the nonlinear interactions leading to the onset of transition. Thus, a similar analysis for the circular cone geometry of the HIFiRE-1 model was deemed useful.

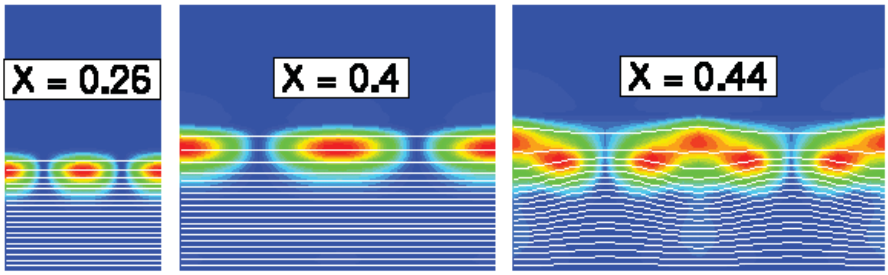

Figure 12. Contours of root mean square (RMS) streamwise velocity fluctuation at three streamwise locations. At each location, the fluctuation amplitude is normalized by the value of its local peak. Blue color denotes zero fluctuations, whereas the red color denotes the peak velocity fluctuations. The background white lines represent contours of streamwise velocity (coming out of paper). The horizontal extent of each plot corresponds to a single azimuthal wavelength of the *n* = 80 mode, which increases along the cone as the local diameter increases.

To enable a follow-on study of laminar flow breakdown due to secondary instabilities, the nonlinear evolution of second mode disturbances was computed using direct numerical simulations (DNS). The DNS code used for this computation has been extensively validated in the context of transition analysis ranging from linear and nonlinear wave propagation [14] to the laminar breakdown phase of transition [15]. The computational grid was based on the prior experience and, even though no grid convergence analysis was performed, is expected to be adequate for tracking the evolution of the second mode. The trajectory point corresponding to t = 21.5 seconds was selected for this simulation and the nonlinear development of the 475 kHz second mode instability, which reaches a peak linear N-factor of 18.3 at this flow condition, was monitored after artificially forcing this mode using a surface actuator at an upstream location close to where this mode first begins to amplify. The nonlinear development of this second mode instability is shown in Fig. 13, wherein the contours of density gradient normal to the wall are plotted as a numerical Schlieren flow visualization. The rope-like contours characteristic of nonlinear second mode disturbances [16] are clearly seen. The linear second mode wave at 475 kHz frequency remains unstable until the end of the cone (i.e., up to X = 1.1 m). On the other hand, the contours from Fig. 13 indicate that nonlinear effects cause this disturbance to reach its peak amplitude just past X = 0.85 m, after which it decays rather rapidly, qualitatively analogous to the cone with concave curvature.

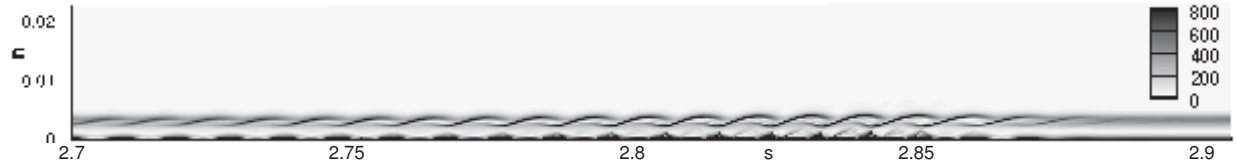

Figure 13. Nonlinear development of 475 kHz second mode instability for conditions at 21.5 seconds into the flight. Flood contours show the normal density gradient in the presence of large amplitude second mode waves. The coordinates s and n correspond to the distance from the nose tip along the cone surface and the wall normal coordinate, respectively. Both coordinates are measured in feet in this figure.

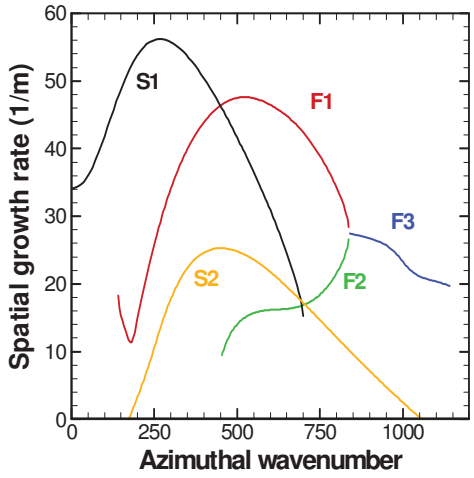

Figure 14. Linear growth rates of secondary instability modes at a selected location (X = 0.846 m). Lines marked with F and S representing fundamental and subharmonic modes, respectively.

The nonlinearly perturbed flow is extracted at X = 0.846 m, based on which local secondary instability computations are carried out. The primary wave RMS amplitude is 7.8% in streamwise velocity fluctuations. Fig. 14 shows the growth rates at different azimuthal wavenumbers for the fundamental and subharmonic modes based on the secondary instability theory. The fundamental mode has higher growth rates in comparison with the subharmonic modes. The unstable spectra span a wide range of azimuthal wavenumbers (n) with peak local growth rate at approximately n = 60 for the fundamental mode. Both types of secondary instability are approximately phase locked with the second mode primary instability. For comparable primary wave amplitudes, these growth rates are comparable to those computed for the compression cone case. At this station the 'S1' subharmonic mode is found to be dominant whereas, in the compression cone case, a fundamental mode has the maximum overall amplification. Conclusions of a similar nature for the present geometry will have to await secondary instability computations at all stations. The growth rate curves in Fig. 14 also indicate coalescence between two branches. Even though the coalescence occurred away from the locally maximum growth rates, it would be essential to examine its global implications. The follow on DNS computations will target this. In addition, the combined evolution of the (primary) secondary mode and the secondary instabilities above will be tracked to understand the details of the transition process and determine whether such mechanisms may be partially amenable to measurement during future flight experiments of a similar nature.

3. CONCLUSIONS

In any transition process, nonlinear mechanisms are ultimately responsible for the breakdown of wave-like disturbances and need to be analyzed to advance transition prediction methods based on higher fidelity methodologies. Secondary instability of 2D/axisymmetric second mode disturbances was examined for a representative set of high-speed boundary layer flows. Unlike in the previous studies, the selection of primary disturbances used for secondary instability analysis was based on their potential relevance to transition in a low disturbance environment and the effects of nonlinearity on the evolution was primary disturbances was accounted for. Computations confirmed the previously known dominance of subharmonic modes at relatively small primary amplitudes. However, for the Purdue Mach 6 compression cone configuration, it was shown that a strong fundamental secondary instability can exist for a range of initial amplitudes of the most amplified second mode disturbance, indicating that the exclusive focus on subharmonic modes in the previous applications of secondary instability theory to second mode primary instability may not have been fully justified. As discussed in [1, 17], however, other factors such as the presence of stationary streamwise vorticity in the flow can easily influence the relative importance of subharmonic and fundamental modes and, therefore, the determination of which mode of secondary instability is likely to dominate in any specific context has to be addressed on a case by case basis using a more complete knowledge of the initial disturbance spectrum within the boundary layer.

ACKNOWLEDGMENT

This work was performed as part of the Aerodynamics, Aerothermodynamics, and Plasma Dynamics (AAP) discipline of the Hypersonics Project of NASA's Fundamental Aeronautics Program (FAP).

REFERENCES

1. Herbert, T., "Secondary Instability of Boundary Layers," *J. Fluid Mech.,* Vol. 20, p. 487, 1988.
2. Ng., L. and Erlebacher, G., "Secondary Instabilities in Compressible Boundary Layers," *Phys. Fluids A* , Vol. 4 (4), pp. 710-26, April 1992.
3. El-Hady, N.M. "Spatial three-dimensional secondary instability of compressible boundary-layer flows," *AIAA J.*, Vol. 29, No. 5, pp. 688-696, 1991.
4. El-Hady, N.M., "Secondary Instability of High-Speed Flows and the Influence of Wall Cooling and Suction," *Phys. Fluids A* , Vol. 4 (4), pp. 727-743, April 1992.
5. Wheaton, B. M., Juliano, T. J., Berridge, D. C., Chou, A., Gilbert, P. L., Casper, K. M., Sheen, L. E. and Schneider, S. P., "Instability and Transition Measurements in the Mach-6 Quiet Tunnel," AIAA Paper 2009-3559, 2009.
6. Kimmel, R. L., Adamczak, D. and DSTO AVD Brisbane Team, "HIFiRE Preliminary Aerothermodynamic Measurements," AIAA Paper 2011-3413, 2011.
7. Li, F. and Choudhari, M., "Spatially Developing Secondary Instabilities and Attachment Line Instability in Supersonic Boundary Layers," AIAA Paper 2008-590, 2008. (also: Li, F. and Choudhari, M., "Spatially Developing Secondary Instabilities in Compressible Swept Airfoil Boundary Layers," *Theoretical and Computational Fluid Dynamics*, Vol. 25, pp. 65-84, 2011)
8. Li, F., Choudhari, M. M., Chang, C.-L., Wu, M. and Greene, P. T., "Development and Breakdown of Görtler Vortices in High Speed Boundary Layers," AIAA Paper 2010-705, 2010.
9. Li, F., Choudhari, M., Chang, C.-L. and White, J., "Analysis of Instabilities in Non-Axisymmetric Hypersonic Boundary Layers over Cones," AIAA Paper 2010-4643, 2010.
10. http://vulcan-cfd.larc.nasa.gov/index.html
11. Chang, C.-L., "Langley Stability and Transition Analysis Code (LASTRAC) Version 1.2 User Manual," *NASA/TM-2004-213233,* 2004.
12. Sivasubramanian, J. and Fasel, H., "Nonlinear Stages of Transition and Breakdown in a Boundary Layer on a Sharp Cone at Mach 6," AIAA Paper 2012-87, 2012.
13. Li, F., Choudhari, M., Chang, C.-L., Kimmel, R., Adamczak, D. and Smith, M., "Transition Analysis for the HIFiRE-1 Flight Experiment," AIAA Paper 2011-3414, 2011.
14. Jiang, L., Chang, C.-L., Choudhari, M. and Liu, C., "Instability-Wave Propagation in Boundary-Layer Flows at Subsonic through Hypersonic Mach Numbers," *Mathematics and Computers in Simulation*, Vol. 65, pp. 469-487, 2004.
15. Jiang, L., Choudhari, M., Chang, C.-L. and Liu, C., "Direct Numerical Simulations of Transition in a Supersonic Boundary Layer," AIAA Paper 2006-3224, 2006.
16. Pruett, C.D. and Chang, C.-L., "Direct Numerical Simulation of Hypersonic Boundary-Layer Flow on a Flared Cone," *Theoretical and Computational Fluid Dynamics*, Vol. 11, No. 1, pp. 49-67, 1998.
17. Singer, B.A., Reed, H.L. and Ferziger, J.H., "The Effects of Streamwise Vortices on Transition in the Plane Channel," *Phys. Fluids A* , Vol. 1 (12), pp. 1960-1971, Dec. 1989